EasyChair Preprint

№ 15631

Improving Accuracy of Ideal-Element Propagation by Manifold Correction

Martin Lara

December 23, 2024

Improving accuracy of ideal-element propagation by manifold correction*

Martin Lara

Scientific Computing and Technological Innovation Center, University of La Rioja
Edificio CCT, C/ Madre de Dios, 53, ES-26006 Logroño, Spain
mlara0@gmail.com

***Abstract* – An algorithm is proposed for improving performance of numerical integration based on Hansen's ideal frame when applied to conservative perturbed Keplerian motion. The procedure relies on the techniques of manifold projection methods, and is computationally inexpensive. The benefits of this approach are illustrated with the main problem of artificial satellite theory, whose variation equations are formulated explicitly in the ideal frame to avoid rotations.**

I. Introduction

Two basic ways of improving the numerical integration of perturbed Keplerian motion include the integration of elements—also called parameters, or constants—rather than coordinates [1, 2], and the use of variable step size distribution along the orbit. Because the elements evolve slowly, their propagation advances with larger step sizes than in the case of coordinates, which, therefore, expedite the numerical integration and reduce the accumulation of numerical errors. The step size regulation adapts the numerical integration to the geometric characteristics of elliptic Keplerian motion, in this way avoiding the use of unnecessarily short step sizes close to apogee. It can be attained either by numerical methods, which is the aim of variable step size numerical solvers [3, 4], or using analytical time-regularization techniques [5, 6, 7, 8]. Moreover, in the common case in which the differential system admits integrals, they can be used to improve the fidelity of the numerical solution either by introducing the integral in the differential system as a coupled control term [9], or in a calibration of the solution obtained after each integration step [10]. The latter technique is usually known as manifold correction or projection [11, 12].

The procedure of manifold projection is seen as dispensable when the numerical integration is approached in elements, as opposite to coordinates, for the stability of the variation-of-parameters approach [13]. However, it is well known that the inaccuracies in the integration of the semimajor axis play a major role in triggering the Lyapunov-type instability that is characteristic of perturbed Keplerian motion. Therefore, we will see that the use of this calibration method may help in preventing the growth of the dominant in-track errors in elements-based integrations too.

The calibration process is illustrated with the numerical integration of the main problem of the Earth artificial satellite theory, which accepts the energy as an integral. More precisely, the variation equations of the main problem are integrated numerically in the classical set of ideal elements [14, 15], which are recognized to shine at numerically integrating perturbed Keplerian motion [16]. The physical time is taken as the independent variable, and the manifold correction is applied to preserve the total energy. Our energy-scaling process affects exclusively the ideal elements related to the representation of the conic in the orbital plane.

For this particular application, the performance of the ideal-elements integration has been leveraged by explicitly reformulating the main problem equations in the ideal frame [17]. In this way, the number of computer operations is drastically reduced by avoiding the need of carrying out repeated rotations between the ideal and space frames, which otherwise would be needed for the evaluation of the right sides of the differential equations at each integration step.

II. The ideal frame algorithm

A typical set of ideal-frame varaibles is composed by the Euler angles (Ω, I, β) that describe the attitude of the ideal frame $(O, \boldsymbol{u}^*, \boldsymbol{v}^*, \boldsymbol{n})$—where $\boldsymbol{n}$ is the direction of the angular momentum vector—with respect to an inertial, departure frame $(O, \boldsymbol{i}, \boldsymbol{j}, \boldsymbol{k})$, and the polar variables $(r, \theta, \dot{r}, \Theta)$, where Θ denotes the specific angular momentum, which describe the motion in the orbital plane. The polar angle θ fixes the position of the orbital frame $(O, \boldsymbol{u}, \boldsymbol{v}, \boldsymbol{n})$, where $\boldsymbol{u}$ denotes the radial direction, with respect to the ideal frame. That is,

$$\boldsymbol{u} = \boldsymbol{u}^* \cos\theta + \boldsymbol{v}^* \sin\theta,$$
$$\boldsymbol{v} = \boldsymbol{v}^* \cos\theta - \boldsymbol{u}^* \sin\theta.$$

*Acknowledgements: Support by the Spanish State Research Agency and the European Regional Development Fund through Project PID2021-123219OB-I00, AEI/ERDF, EU, is recognized.

To guarantee that the frame is ideal, the variation of the Euler angles must fulfill the equations

$$\begin{aligned}\sin I\,\dot\Omega &= (r/\Theta)\mathcal{N}\sin(\theta+\beta),\\ \dot I &= (r/\Theta)\mathcal{N}\cos(\theta+\beta),\\ \dot\beta &= -\dot\Omega\cos I,\end{aligned}$$

where $\mathcal{N}=\boldsymbol{P}\cdot\boldsymbol{n}$, and $\boldsymbol{P}$ is the disturbing acceleration of the Keplerian motion, cf. [18]. Moreover, to avoid singularities, the attitude is rather described by the redundant set of Euler parameters [18]

$$\begin{aligned}\lambda_1 &= \sin\tfrac{1}{2}I\cos\tfrac{1}{2}(\Omega-\beta),\\ \lambda_2 &= \sin\tfrac{1}{2}I\sin\tfrac{1}{2}(\Omega-\beta),\\ \lambda_3 &= \cos\tfrac{1}{2}I\sin\tfrac{1}{2}(\Omega+\beta),\\ \lambda_4 &= \cos\tfrac{1}{2}I\cos\tfrac{1}{2}(\Omega+\beta).\end{aligned}\tag{1}$$

To obtain a complete set of variation-of-parameters equations, the integration of the polar variables is customarily replaced by the integration of a time element and the three hodographic velocities

$$\kappa=\frac{\mu}{\Theta}\boldsymbol{e}\cdot\boldsymbol{u}^*,\qquad \sigma=\frac{\mu}{\Theta}\boldsymbol{e}\cdot\boldsymbol{v}^*,\qquad \zeta=\frac{\mu}{\Theta},\tag{2}$$

where μ is the gravitational parameter and $\boldsymbol{e}$ denotes the eccentricity vector [14, 16]. Alternatively, the integration of the time element can be replaced by that of the polar angle θ, in this way avoiding the constraint of the variation equations to the case of bounded motion.

Then, we arrive to the variation equations

$$\begin{aligned}\dot\theta &= \mu/(r^2\zeta),\\ \dot\kappa &= (1+r/p)\mathcal{T}\cos\theta+\mathcal{R}\sin\theta,\\ \dot\sigma &= (1+r/p)\mathcal{T}\sin\theta-\mathcal{R}\cos\theta,\\ \dot\zeta &= -(r/p)\mathcal{T},\\ \dot\lambda_1 &= \tfrac{1}{2}(1/\zeta)(r/p)\mathcal{N}(\lambda_4\cos\theta-\lambda_3\sin\theta),\\ \dot\lambda_2 &= \tfrac{1}{2}(1/\zeta)(r/p)\mathcal{N}(\lambda_4\sin\theta+\lambda_3\cos\theta),\\ \dot\lambda_3 &= \tfrac{1}{2}(1/\zeta)(r/p)\mathcal{N}(\lambda_1\sin\theta-\lambda_2\cos\theta),\\ \dot\lambda_4 &= -\tfrac{1}{2}(1/\zeta)(r/p)\mathcal{N}(\lambda_1\cos\theta+\lambda_2\sin\theta),\end{aligned}\tag{3}$$

in which $\mathcal{R}=\boldsymbol{P}\cdot\boldsymbol{u}$, $\mathcal{T}=\boldsymbol{P}\cdot\boldsymbol{v}$, $p=\Theta^2/\mu$ is the parameter of the conic, and

$$\frac{p}{r}=1+\frac{\kappa}{\zeta}\cos\theta-\frac{\sigma}{\zeta}\sin\theta,\tag{4}$$

$$\dot r=\kappa\sin\theta-\sigma\cos\theta,\tag{5}$$

Denoting $\boldsymbol{x}$ the Cartesian coordinates and $\dot{\boldsymbol{x}}$ the corresponding velocities, the initial conditions needed for integrating Eq. (3) for given $\boldsymbol{x}_0=\boldsymbol{x}(t_0)$, $\dot{\boldsymbol{x}}_0=\dot{\boldsymbol{x}}(t_0)$, are computed through the sequence: $r_0=\|\boldsymbol{x}_0\|$, $\boldsymbol{G}_0=\boldsymbol{x}_0\times\dot{\boldsymbol{x}}_0$, $\Theta_0=\|\boldsymbol{G}_0\|$, and $p_0=\Theta_0^2/\mu$. Then,

$$\boldsymbol{u}_0=\frac{\boldsymbol{x}_0}{r_0},\qquad \boldsymbol{n}_0=\frac{\boldsymbol{G}_0}{\Theta_0},\qquad \boldsymbol{v}_0=\boldsymbol{n}_0\times\boldsymbol{u}_0,$$

and

$$\begin{aligned}\lambda_{4,0} &= \tfrac{1}{2}(1+\boldsymbol{u}_0\cdot\boldsymbol{i}+\boldsymbol{v}_0\cdot\boldsymbol{j}+\boldsymbol{n}_0\cdot\boldsymbol{k})^{1/2},\\ \lambda_{1,0} &= \tfrac{1}{4}(\boldsymbol{v}_0\cdot\boldsymbol{k}-\boldsymbol{n}_0\cdot\boldsymbol{j})/\lambda_{4,0},\\ \lambda_{2,0} &= \tfrac{1}{4}(\boldsymbol{n}_0\cdot\boldsymbol{i}-\boldsymbol{u}_0\cdot\boldsymbol{k})/\lambda_{4,0},\\ \lambda_{3,0} &= \tfrac{1}{4}(\boldsymbol{u}_0\cdot\boldsymbol{j}-\boldsymbol{v}_0\cdot\boldsymbol{i})/\lambda_{4,0},\end{aligned}$$

cf. [19]. Finally, $\zeta_0=\mu/\Theta_0$, and the customary choice $\theta_0=0$ results in

$$\kappa_0=\frac{\Theta_0}{r_0}-\frac{\Theta_0}{p_0},\qquad \sigma_0=-\dot r_0=-\boldsymbol{u}_0\cdot\dot{\boldsymbol{x}}_0.$$

At each integration step, the polar coordinates are computed using Eqs. (4)–(5), from which

$$\boldsymbol{x}=\mathbf{M}\begin{bmatrix}r\cos\theta\\ r\sin\theta\\ 0\end{bmatrix},\quad \dot{\boldsymbol{x}}=\mathbf{M}\begin{bmatrix}\dot r\cos\theta-(\Theta/r)\sin\theta\\ \dot r\sin\theta+(\Theta/r)\cos\theta\\ 0\end{bmatrix},$$

where the coefficients of the rotation matrix from the ideal to the inertial frame $\mathbf{M}$ are detailed in Table 1.

$i\setminus j$	1	2	3
1	$1-2(\lambda_2^2+\lambda_3^2)$	$2(\lambda_1\lambda_2-\lambda_4\lambda_3)$	$2(\lambda_1\lambda_3+\lambda_2\lambda_4)$
2	$2(\lambda_1\lambda_2+\lambda_4\lambda_3)$	$1-2(\lambda_1^2+\lambda_3^2)$	$2(\lambda_2\lambda_3-\lambda_1\lambda_4)$
3	$2(\lambda_1\lambda_3-\lambda_2\lambda_4)$	$2(\lambda_2\lambda_3+\lambda_1\lambda_4)$	$1-2(\lambda_1^2+\lambda_2^2)$

Table 1: Coefficients of the rotation matrix $\mathbf{M}=(M_{i,j})$.

III. Main problem in ideal elements

The main problem of artificial satellite theory stems from the truncation of the gravitational potential to the only contribution of the zonal harmonic of the second degree [20]. That is, using spherical coordinates (r,φ,λ), the main problem potential is

$$\mathcal{V}=-\frac{\mu}{r}+V,\quad V=J_2\frac{\mu}{r}\frac{R_\oplus^2}{r^2}\frac{1}{2}\left(3\sin^2\varphi-1\right),\tag{6}$$

where $R_\oplus$ is the equatorial radius of the attracting body, and J_2 is the zonal harmonic coefficient of degree 2.

The disturbing acceleration $\boldsymbol{P}=-\nabla_{\boldsymbol{x}}V$ stemming from Eq. (6) is computed in spherical coordinates. Namely, $\partial V/\partial\lambda\equiv 0$ for the axial symmetry of the main problem, and $\boldsymbol{P}=-(\partial V/\partial r)\boldsymbol{u}-(1/r)(\partial V/\partial\varphi)\hat{\boldsymbol{\varphi}}$, where $\hat{\boldsymbol{\varphi}}$ is a unit vector in the latitude direction, and

$$\begin{aligned}\frac{\partial V}{\partial r} &= -J_2\frac{\mu}{r^2}\frac{R_\oplus^2}{r^2}\frac{3}{2}\left(3\sin^2\varphi-1\right),\\ \frac{\partial V}{\partial\varphi} &= J_2\frac{\mu}{r}\frac{R_\oplus^2}{r^2}3\sin\varphi\cos\varphi.\end{aligned}$$

The decomposition of the unit vector $\boldsymbol{k}$ in the meridian plane is rewritten as $\hat{\boldsymbol{\varphi}}\cos\varphi = \boldsymbol{k} - \boldsymbol{u}\sin\varphi$, which, besides, shows that $\sin\varphi = \boldsymbol{k}\cdot\boldsymbol{u}$. Therefore,

$$\boldsymbol{P} = \frac{3}{2}J_2\frac{\mu}{r^2}\frac{R_\oplus^2}{r^2}\left\{\left[5(\boldsymbol{k}\cdot\boldsymbol{u})^2 - 1\right]\boldsymbol{u} - 2(\boldsymbol{k}\cdot\boldsymbol{u})\,\boldsymbol{k}\right\},$$

whose components in the orbital frame are

$$\begin{bmatrix}\mathcal{R}\\ \mathcal{T}\\ \mathcal{N}\end{bmatrix} = -3J_2\frac{\mu}{r^2}\frac{R_\oplus^2}{r^2}\begin{bmatrix}\frac{1}{2} - \frac{3}{2}(\boldsymbol{k}\cdot\boldsymbol{u})^2\\ (\boldsymbol{k}\cdot\boldsymbol{v})(\boldsymbol{k}\cdot\boldsymbol{u})\\ (\boldsymbol{k}\cdot\boldsymbol{n})(\boldsymbol{k}\cdot\boldsymbol{u})\end{bmatrix}, \qquad (7)$$

cf. [17], which only depend on r and the projections of $\boldsymbol{k}$ in the orbital frame. Namely, $\boldsymbol{k} = R_3(\theta)\mathbf{M}(t)^\tau\,(0,0,1)^\tau$, where R_3 denotes the rotation matrix about $\boldsymbol{n}$. Therefore,

$$\begin{bmatrix}\boldsymbol{k}\cdot\boldsymbol{u}\\ \boldsymbol{k}\cdot\boldsymbol{v}\\ \boldsymbol{k}\cdot\boldsymbol{n}\end{bmatrix} = \begin{bmatrix}\frac{1}{2}M_{3,1}\cos\theta + M_{3,2}\sin\theta\\ M_{3,2}\cos\theta - \frac{1}{2}M_{3,1}\sin\theta\\ M_{3,3}\end{bmatrix}, \qquad (8)$$

with coefficients $M_{3,j}$, in the third row of Table 1.

IV. Manifold correction

The main problem admits the energy $E = \frac{1}{2}\dot{\boldsymbol{x}}\cdot\dot{\boldsymbol{x}} - (\mu/r) + V$ and the third component of the angular momentum vector $H = \Theta\cos I$ as integrals. Neither of them will be constant in practice due to the accumulation of numerical errors. Conversely, we can use their known values $E = E_0$, $H = H_0$, obtained from the initial conditions, to force the numerically integrated solution to lie on the proper manifolds [10]. In particular, the energy is written in the form

$$E = -\frac{\mu}{2a}\left\{1 + J_2\frac{a}{r}\frac{R_\oplus^2}{r^2}\left[1 - 3(\boldsymbol{k}\cdot\boldsymbol{u})^2\right]\right\},$$

which shows that the more important element to correct is the semimajor axis $a = p/(1-e^2)$, where $e = \|\boldsymbol{e}\|$. The simple scaling

$$\tilde{a} = -\frac{\mu}{2E_0}\left\{1 + J_2\frac{a_m}{r_m}\frac{R_\oplus^2}{r_m^2}\left[1 - 3(\boldsymbol{k}\cdot\boldsymbol{u}_m)^2\right]\right\},$$

where m denotes the integration step, will notably improve the preservation of the energy, cf. [21]. On the other hand, a does not pertain to the set of ideal elements in Eq. (3). According to Eq. (2), it is written in terms of the ideal elements as $a = \mu/(\zeta^2 - \kappa^2 - \sigma^2)$, thus showing the convenience of scaling the three hodographic velocities by the same factor as a; namely $q_m = \tilde{a}/a_m$. That is, at each step m of the numerical integration, we replace the numerically integrated values κ_m, σ_m, and ζ_m, by the scaled ones

$$\tilde{\kappa} = \kappa_m q_m, \qquad \tilde{\sigma} = \sigma_m q_m, \qquad \tilde{\zeta} = \zeta_m q_m. \qquad (9)$$

Writing the polar component of the angular momentum as $H = \Theta(1 - 2\sin^2\frac{1}{2}I)$, and on account of Eq. (1), we obtain $H = \Theta\left(\lambda_3^2 + \lambda_4^2 - \lambda_1^2 - \lambda_2^2\right)$, which suggests an analogous scaling of λ_i to guarantee its preservation $H = H_0$. Note, however, that this new scaling should be done with great care in order to not contravene the geometric constrain $\sum_{i=1}^4 \lambda_i^2 = 1$.

V. Example illustration

An example is provided to illustrate the effects of the energy-scaling calibration of the hodographic velocities. In the simulations, the parameters defining the potential are particularized for the Earth. That is, $\mu = 398600.4415\,\mathrm{km}^3/\mathrm{s}^2$, $R_\oplus = 6378.1363\,\mathrm{km}$, and $J_2 = 0.001082634$.

We focus on the low eccentricity orbit with initial elements in Table 2, which we propagate for a one-month. The true, reference orbit was computed from the numerical integration of the J_2 problem in Cartesian coordinates in extended precision, which we then truncate to the 16 significant figures of the standard machine precision. We checked that this truncation of the reference orbit routinely preserves 15 significant figures in the computation of the energy integral, and the 16 figures of the third component of the angular momentum vector are preserved most times.

Orbital elements		Ideal elements (internal units)	
a	6878.14 km	λ_1	-0.386404272277476
e	0.001	λ_2	-0.644411685305790
I	97.42°	λ_3	-0.623505510971901
Ω	168.16°	κ	$8.655216828077350\cdot10^{-4}$
ω	270°	σ	$-5.008699024326435\cdot10^{-4}$
M	30°	ζ	1.000000499999096

Table 2: Initial conditions of the test orbit; $\theta = 0$ and $\lambda_4 = (1 - \lambda_1^2 - \lambda_2^2 - \lambda_3^2)^{1/2}$.

Ideal-frame integrations were carried out with and without energy-scaling control. Their respective intrinsic errors, as well as the errors in the preservation of the energy along the propagation interval, were computed with respect to the reference solution. The time-histories of the intrinsic errors, as well as the relative errors in the preservation of the energy are depicted in Fig. 1 for the standard, non-controlled, ideal-element propagation, and in Fig. 2 for the case of the energy-scaling control.

Thus, as shown by comparison of the upper plots of Figs. 1 and 2, the energy-scaling control is quite effective, yielding negligible relative errors of $\mathcal{O}(10^{-15})$ after control. Along-track errors are reduced by about one order of magnitude with the energy scaling: from about half mm without control at the end of the 30-day interval (lower plot of Fig. 1) to a maximum of about half tenth

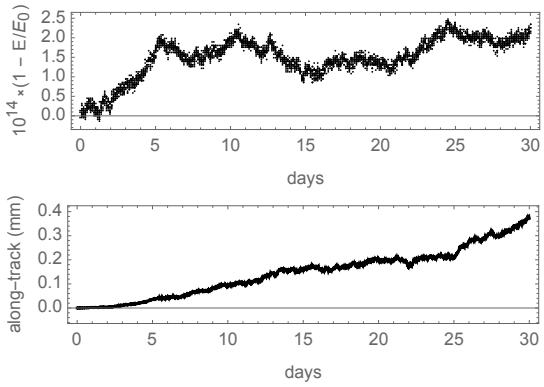

Figure 1: Errors of the test orbit without energy-scaling.

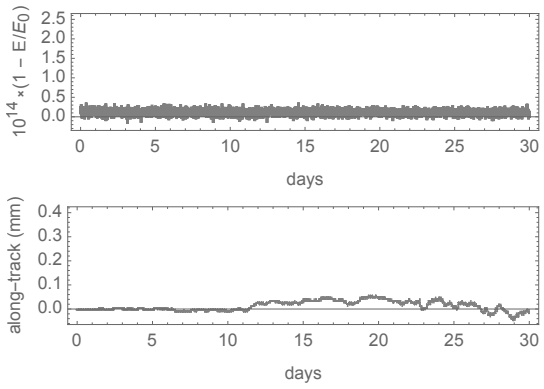

Figure 2: Errors of the test orbit with energy-scaling.

of mm when the energy scaling is applied (lower plot of Fig. 2). Radial and cross-track errors remain very small in both different integrations, but since they suffer the coupling with along-track errors it can be checked that they clearly improve in the case of energy scaling.

VII. References

[1] R.H. Battin. *An Introduction to the Mathematics and Methods of Astrodynamics*. AIAA, Inc., Reston, Virginia, 1999.

[2] A.E. Roy. *Orbital Motion*. Institute of Physics Publishing, Bristol (UK), 2005.

[3] E. Fehlberg. *Classical Fifth-, Sixth-, Seventh- and Eighth-Order Runge-Kutta Formulas with Stepsize Control*. NASA TR R-287, Marshall Space Flight Center, Huntsville, Alabama, October 1968.

[4] L.F. Shampine and M.K. Gordon. *Computer Solution of Ordinary Differential Equations*. Freeman and Co., San Francisco, 1975.

[5] H. Sperling. "Computation of Keplerian conic sections." *ARS Journal*, 31(5):660–661, 1961.

[6] C.A. Burdet. "Theory of Kepler motion: the general perturbed two body problem." *ZAMP*, 19(2):345–368, March 1968.

[7] E.L. Stiefel and G. Scheifele. *Linear and Regular Celestial Mechanics*. Springer-Verlag, 1971.

[8] J.M. Ferrándiz. "Linearization in special cases of perturbed Keplerian motions." *Celest. Mech.*, 39:23–31, 1986.

[9] J. Baumgarte. "Stabilization of constraints and integrals of motion in dynamical systems." *Comput. Methods Appl. Mech. Eng.*, 1(1):1–16, 1972.

[10] P.E. Nacozy. "The use of integrals in numerical integrations of the n-body problem." *Astrophys. & Space Sci.*, 14(1):40–51, 1971.

[11] T. Fukushima. "Efficient orbit integration by manifold correction methods." *Ann. N.Y. Acad. Sci.*, 1065(1):37–43, 2005.

[12] E. Hairer, C. Lubich, and G. Wanner. *Geometric Numerical Integration. Structure-Preserving Algorithms for Ordinary Differential Equations*. Springer-Verlag, 2006.

[13] T. Fukushima. "Further simplification of the manifold correction method for orbit integration." *Astron. J.*, 128(3):1446–1454, 2004.

[14] A. Deprit. "Ideal elements for perturbed Keplerian motions." *J. Res. Natl. Bur. Stand.*, 79:1–15, 1975.

[15] M. Lara. "Note on the ideal frame formulation." *Celest. Mech. Dyn. Astron*, 129:137–151, 2017.

[16] M. Lara and H. Urrutxua. "Revisiting Hansen's ideal frame propagation with special perturbations. 1: Basic algorithms for osculating elements." *Universe*, 9(11), 2023.

[17] H. Urrutxua, M. Sanjurjo-Rivo, and J. Peláez. "DROMO propagator revisited." *Celest. Mech. Dyn. Astron*, 124:1–31, 2016.

[18] P. Musen. "Modified formulae for Hansen's special perturbations." *Astron. J.*, 63:426–429, 1958.

[19] M.A. Sharaf, M.E.-S. Awad, and S.A.S.A. Najmuldeen. "The motion of artificial satellites in the set of Eulerian redundant parameters." *Earth Moon Planets*, 55(1):21–44, 1991.

[20] D. Brouwer. "Solution of the problem of artificial satellite theory without drag." *Astron. J.*, 64:378–397, 1959.

[21] J.V. Breakwell and J. Vagners. "On error bounds and initialization in satellite orbit theories." *Celest. Mech.*, 2:253–264, 1970.